Phase-sensitive imaging of tissue acoustic vibrations using spectrally encoded interferometry

Ovadia Ilgayev and Dvir Yelin*

Faculty of Biomedical Engineering, Technion—Israel Institute of Technology, Haifa 32000, Israel
**yelin@bm.technion.ac.il*

Abstract: Acoustic vibrations in tissue are often difficult to image, requiring high-speed scanning, high sensitivity and nanometer-scale axial resolution. Here we use spectrally encoded interferometry to measure the vibration pattern of two-dimensional surfaces, including the skin of a volunteer, at nanometric resolution, without the need for rapid lateral scanning and with no prior knowledge of the driving acoustic waveform. Our results demonstrate the feasibility of this technique for measuring tissue biomechanics using simple and compact imaging probes.

OCIS codes: (170.2150) Endoscopic imaging; (170.3340) Laser Doppler velocimetry; (120.7280) Vibration analysis; (170.6935) Tissue characterization.

References and Links

1. A. M. Huber, C. Schwab, T. Linder, S. J. Stoeckli, M. Ferrazzini, N. Dillier, and U. Fisch, "Evaluation of Eardrum Laser Doppler Interferometry as a Diagnostic Tool," Laryngoscope **111**(3), 501–507 (2001).
2. J. J. Rosowski, H. H. Nakajima, and S. N. Merchant, "Clinical utility of laser-Doppler vibrometer measurements in live normal and pathologic human ears," Ear Hear. **29**(1), 3–19 (2008).
3. K. R. Whittemore, Jr., S. N. Merchant, B. B. Poon, and J. J. Rosowski, "A normative study of tympanic membrane motion in humans using a laser Doppler vibrometer (LDV)," Hear. Res. **187**(1-2), 85–104 (2004).
4. E. W. Chang, J. B. Kobler, and S. H. Yun, "Subnanometer optical coherence tomographic vibrography," Opt. Lett. **37**(17), 3678–3680 (2012).
5. G. Liu, M. Rubinstein, A. Saidi, W. Qi, A. Foulad, B. Wong, and Z. Chen, "Imaging vibrating vocal folds with a high speed 1050 nm swept source OCT and ODT," Opt. Express **19**(12), 11880–11889 (2011).
6. A. Burkhardt, L. Kirsten, M. Bornitz, T. Zahnert, and E. Koch, "Investigation of the human tympanic membrane oscillation ex vivo by Doppler optical coherence tomography," J. Biophotonics doi: 10.1002/jbio.201200186 (2012).
7. E. W. Chang, J. B. Kobler, and S. H. Yun, "Triggered optical coherence tomography for capturing rapid periodic motion," Sci. Rep. **1**, 48 (2011).
8. J. T. Cheng, A. A. Aarnisalo, E. Harrington, M. S. Hernandez-Montes, C. Furlong, S. N. Merchant, and J. J. Rosowski, "Motion of the surface of the human tympanic membrane measured with stroboscopic holography," Hear. Res. **263**(1-2), 66–77 (2010).
9. J. J. Rosowski, I. Dobrev, M. Khaleghi, W. Lu, J. T. Cheng, E. Harrington, and C. Furlong, "Measurements of three-dimensional shape and sound-induced motion of the chinchilla tympanic membrane," Hear. Res. **301**, 44–52 (2013).
10. G. J. Tearney, R. H. Webb, and B. E. Bouma, "Spectrally encoded confocal microscopy," Opt. Lett. **23**(15), 1152–1154 (1998).
11. D. Yelin, I. Rizvi, W. M. White, J. T. Motz, T. Hasan, B. E. Bouma, and G. J. Tearney, "Three-dimensional miniature endoscopy," Nature **443**(7113), 765 (2006).
12. D. Yelin, B. E. Bouma, J. J. Rosowsky, and G. J. Tearney, "Doppler imaging using spectrally-encoded endoscopy," Opt. Express **16**(19), 14836–14844 (2008).
13. K. Goda, A. Mahjoubfar, C. Wang, A. Fard, J. Adam, D. R. Gossett, A. Ayazi, E. Sollier, O. Malik, E. Chen, Y. Liu, R. Brown, N. Sarkhosh, D. Di Carlo, and B. Jalali, "Hybrid dispersion laser scanner," Sci. Rep. **2**, 445 (2012).
14. M. Merman, A. Abramov, and D. Yelin, "Theoretical analysis of spectrally encoded endoscopy," Opt. Express **17**(26), 24045–24059 (2009).
15. R. Onodera, H. Watanabe, and Y. Ishii, "Interferometric phase-measurement using a one-dimensional discrete hilbert transform," Opt. Rev. **12**(1), 29–36 (2005).

#191498 - $15.00 USD Received 31 May 2013; revised 19 Jul 2013; accepted 19 Jul 2013; published 14 Aug 2013

16. Y. Zhao, Z. Chen, C. Saxer, S. Xiang, J. F. de Boer, and J. S. Nelson, "Phase-resolved optical coherence tomography and optical Doppler tomography for imaging blood flow in human skin with fast scanning speed and high velocity sensitivity," Opt. Lett. **25**(2), 114–116 (2000).
17. R. S. Christian, R. E. Davis, A. Tubis, C. A. Anderson, R. I. Mills, and T. D. Rossing, "Effects of air loading on timpani membrane vibrations," J. Acoust. Soc. Am. **76**(5), 1336–1345 (1984).
18. J. Bishop, G. Poole, M. Leitch, and D. B. Plewes, "Magnetic resonance imaging of shear wave propagation in excised tissue," J. Magn. Reson. Imaging **8**(6), 1257–1265 (1998).
19. A. P. Sarvazyan, O. V. Rudenko, S. D. Swanson, J. B. Fowlkes, and S. Y. Emelianov, "Shear wave elasticity imaging: a new ultrasonic technology of medical diagnostics," Ultrasound Med. Biol. **24**(9), 1419–1435 (1998).
20. S. Chen, M. Fatemi, and J. F. Greenleaf, "Quantifying elasticity and viscosity from measurement of shear wave speed dispersion," J. Acoust. Soc. Am. **115**(6), 2781–2785 (2004).
21. A. Manduca, T. E. Oliphant, M. A. Dresner, J. L. Mahowald, S. A. Kruse, E. Amromin, J. P. Felmlee, J. F. Greenleaf, and R. L. Ehman, "Magnetic resonance elastography: non-invasive mapping of tissue elasticity," Med. Image Anal. **5**(4), 237–254 (2001).
22. P. G. Stelmachowicz, K. A. Beauchaine, A. Kalberer, and W. Jesteadt, "Normative thresholds in the 8- to 20-kHz range as a function of age," J. Acoust. Soc. Am. **86**(4), 1384–1391 (1989).
23. C. Boudoux, S. Yun, W. Oh, W. White, N. Iftimia, M. Shishkov, B. Bouma, and G. Tearney, "Rapid wavelength-swept spectrally encoded confocal microscopy," Opt. Express **13**(20), 8214–8221 (2005).

1. Introduction

Noncontact techniques for measuring acoustic vibrations are potentially important tools for clinical diagnosis, providing valuable information on tissue mechanical properties and its response to acoustic stimuli. Using a single laser beam in an interferometric configuration, laser Doppler vibrometry [1–3] is well suited for high-sensitivity measurements of acoustic vibrations of a single point in an object, allowing high-sensitivity measurements of sub-nanometer axial displacements. Measuring the full vibrational patterns of a two-dimensional surface requires knowledge of not only the frequency and amplitude of the wave, but also of the relative phases between different surface locations. Using low coherence interferometry with phase sensitivity, optical coherence tomography (OCT) has been demonstrated useful for capturing volumetric snapshots of vibrating samples using point-by-point scanning and phase synchronization algorithms between the scanning and the excitation acoustic waveforms [4–7]. Single point measurements, however, tend to be time consuming and often require a complex lateral scanning mechanism. Moreover, occasional tissue or probe movements may cause difficulty in stitching the relative phases between adjacent points, leading to difficult and often unreliable reconstruction of the full vibration pattern. Recently, phase-sensitive imaging of two-dimensional surface vibrations was demonstrated using wide-field interferometry and gated pulse illumination [8, 9]; measuring the vibration patterns of excised tympanic membranes, using this technique, has revealed complex vibration modes and traveling waves within the membrane at a wide range of frequencies.

Evidently, capturing fast and dynamic processes such as acoustic vibrations is challenging when using systems that require beam scanning. This difficulty could be addressed using encoding techniques such as spectrally encoded imaging, in which spatial scanning is replaced by spatial encoding of lateral sample locations, using wavelengths from a broadband or a wavelength-swept source. With no need for rapid scanning mechanisms, this approach allows using compact imaging probes that could be handheld or access hard-to-reach regions within the body. In previous work, spectrally encoded endoscopy (SEE) [10, 11] has been demonstrated capable of mapping acoustic vibrations [12] of rigid surfaces (middle ear ossicles) using a single-fiber endoscopic probe placed at the sample arm of a Michelson interferometer. More recently, a single-shot measurement of the entire surface of a vibrating membrane was demonstrated using two-dimensional spectral encoding of ultrashort laser pulses in conjunction with a long dispersive optical fiber and acousto-optic delay scanning [13].

In this work, we propose and demonstrate the measurement of a two-dimensional vibration pattern of tissue surfaces using spectral encoding in a single lateral dimension and slow scanning in the orthogonal dimension, without necessitating the use of ultrashort pulses.

#191498 - $15.00 USD Received 31 May 2013; revised 19 Jul 2013; accepted 19 Jul 2013; published 14 Aug 2013

By analyzing relative spectral phases that correspond to nanometric axial displacements, the vibration patterns of various flexible surfaces, including a paper card, a rubber membrane and the skin of a human volunteer, were imaged at a wide range of acoustic frequencies with no temporal gating or prior knowledge of the driving acoustic waveform. Due to its simplicity and ease-of-use, the technique could potentially be applied for various *in vivo* applications that call for accurate evaluation of tissue mechanical properties and its response to various acoustic stimuli.

2. Experimental setup

2.1 System configuration

The spectrally encoded interferometric imaging system, shown schematically in Fig. 1, consisted of a broadband titanium sapphire oscillator (Femtolasers Rainbow, 200 nm bandwidth, 800 nm center wavelength) coupled to a 50/50 single-mode optical fiber coupler within a Michelson interferometer arrangement. The sample arm of the interferometer consisted of a collimating lens (L1) a single-axis galvanometric scanner, a 1200 lines/mm transmission diffraction grating (G), and a focusing lens (L2, 75 mm focal length). The resulting spectral line (x axis) was scanned in the *y* axis, resulting in a lateral field of view of approximately 20 mm × 20 mm with approximately 680 × 680 resolvable points [14]. The reference arm of the interferometer included a collimating lens (L3), a mirror mounted on a linear translation stage, and a neutral density (ND) filter for adjusting the reference power. Spectral interferograms of the reflected light from the sample and the reference arms were recorded using a custom-built spectrometer, comprised of a collimating lens, a 1800 lines/mm transmission diffraction grating, a focusing lens (Nikon, AF Nikkor, 85 mm focal length) and a high-speed line CCD camera (Sprint spL4096-70k, Basler Vision, 4096 pixels, 70 kHz maximum line rate). The spectral resolution of the spectrometer was approximately 0.1 nm, 5-times higher than the spectral resolution at the sample (0.5 nm). Nonlinearities in the wavelength-to-space mapping have resulted in a small (5.1%) image distortion near the edges of the field of view. Two polarization controllers (PC) were used at the sample and reference arms for increasing interference contrast.

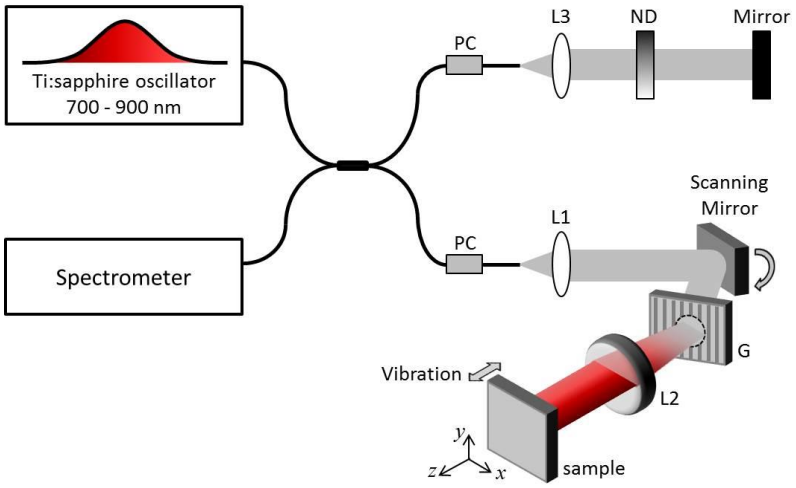

Fig. 1. Schematic of the spectrally encoded imaging system. PC – polarization controller, G – diffraction grating, ND – neutral density filter, L1, L2, L3 - achromatic lenses.

#191498 - $15.00 USD Received 31 May 2013; revised 19 Jul 2013; accepted 19 Jul 2013; published 14 Aug 2013

2.2 Data processing

An initial system calibration was obtained by continuously imaging a single lateral line (no y-axis scanning) on the flat front surface of a piezoelectric crystal that was driven by a single harmonic waveform. For each sample location x_i encoded by a fractional bandwidth δk and centered at an angular wavenumber k_i, the spectral interferogram recorded by the spectrometer at time t is given by:

$$I_k\left(k \in \left[k_i - \frac{\delta k}{2}, k_i + \frac{\delta k}{2}\right]\right) = |E_r|^2 + |E_i|^2 + 2E_r E_i \cos\left(2k\left[z_r - z\left(k_i;t\right)\right]\right), \qquad (1)$$

where E_r denotes the reference field amplitude, E_i denotes the sample field amplitude at location x_i, k denotes the angular wavenumber, and z_r and z denote the optical path lengths of the reference and sample arms, respectively.

Following background subtraction and division by the coefficient of the cosine term in Eq. (1), the argument $\varphi_i = 2k[z_r\text{-}z(k_i,t_i)]$ could now be extracted from the recorded interferogram using the Hilbert transform [15] according to:

$$\varphi_i = \tan^{-1}\left[\frac{H\left\{I_{\cos}\left(k,t\right)\right\}}{I_{\cos}\left(k,t\right)}\right], \qquad (2)$$

where H denotes the Hilbert transform and $I_{\cos}$ is the cosine term in Eq. (1). Finally, the axial sample displacement Δz_i between two subsequent spectral acquisitions could be retrieved using [16]

$$\Delta z_i = \frac{\varphi_i\left(t+dt\right) - \varphi_i\left(t\right)}{2k_i}, \qquad (3)$$

where dt denotes the time difference between subsequent spectral acquisitions, and we assume that the line acquisition rate dt^{-1} is larger than twice the measured acoustic frequency, i.e. $\varphi_i(t + dt)\text{-}\varphi_i(t)<\pi$. The process of calculating the axial displacement of the vibrating crystal surface is summarized in Fig. 2(a).

In order to measure the vibration of a non-rigid object, a small piece of white paper card was attached to the surface of a piezoelectric actuator, while the field of view was adjusted [Fig. 2(b)] so that its left-hand part (0 < x < 6 mm) covered the region of the card that was forced to move with the crystal, while the right-hand part (6 mm < x < 11 mm) was free to move in the z axis. The piezoelectric crystal was driven by a 300 Hz harmonic waveform. The (spatially) averaged maximum displacements at 0<x<6 mm were measured as 25 ± 12 nm and 405 ± 7 nm for ± 300 mV and ± 3.5 V driving voltage amplitudes, respectively, which correlate well with the predicted displacement according to the piezoelectric crystal specifications (± 406 nm and ± 35 nm, respectively). For oversampling the phase differences during the periodic motion, the line (4096 pixels) rate of the camera was 10 kHz, resulting in 33 lines per single vibration cycle, where spectral windows comprised of 32 pixels were used for recording the spectral interferograms that correspond to individual sample locations. Solid (dashed) curves in Fig. 2(b) correspond to the location closest to (most distant from) the lens. The full axial motion of the card is presented in 'Media 1' and 'Media 2' for the driving amplitudes of ± 3.5 V and ± 300 mV, respectively. The smallest measurable displacement (and thus the resolution of the system for small amplitudes) was approximately 3 nm, estimated by calculating the noise floor for zero voltage amplitudes of the driving waveforms.

#191498 - $15.00 USD Received 31 May 2013; revised 19 Jul 2013; accepted 19 Jul 2013; published 14 Aug 2013

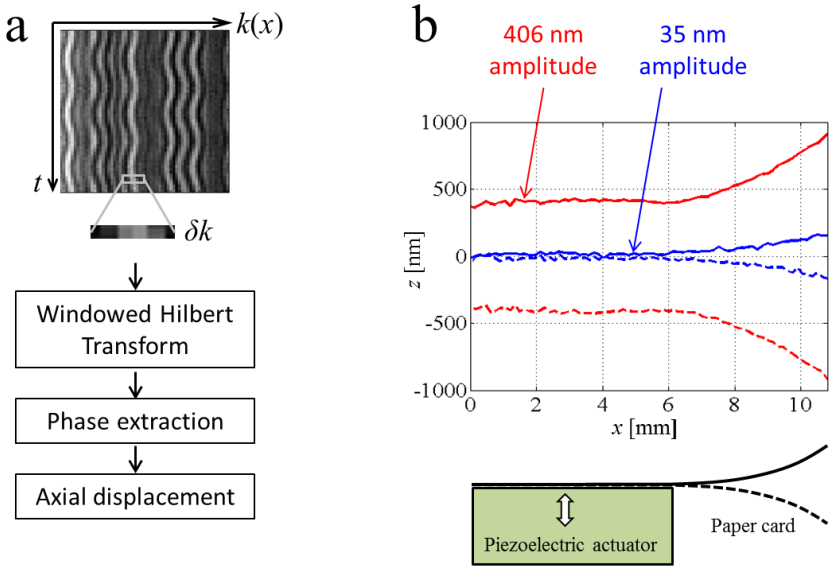

Fig. 2. (a) Calculating axial sample displacement from the raw interferometric data. The grey rectangle corresponds to the fractional bandwidth reflected from a single resolvable point on the sample. (b) Axial displacement of a single lateral line on the surface of a paper card attached to a piezoelectric actuator. Red and blue curves denote positions of extremum sample displacements. Solid (dashed) curves correspond to maximum (minimum) axial card displacements. See the full sample motion during a single oscillation period (3.33 ms total duration) in movies Media 1 and Media 2.

3. Results

In order to demonstrate imaging of two-dimensional vibration patterns of a flexible surface, a small earphone was inserted into a hollow 18-mm-diameter cylindrical tube, whose front end was covered by a rubber membrane [Fig. 3(a)].

The vibrating membrane was scanned by the spectral line (x-axis) in the y-axis at a slow speed of 2.5 mm/s that enabled oversampling of 100 spectral interferograms per sample location. Acquisition line rates were adjusted for each driving frequency to allow sufficient temporal oversampling (25-30 spectral acquisitions per oscillation period). By assuming surface continuity and uniform frequency distribution across the sample, the full two-dimensional image of the surface vibrations was constructed by matching the phases between successive lines. The vibration amplitude at each sample location was also calculated, as well as the local frequency that was determined from the raw data, without relying on prior knowledge of the driving acoustic wave.

Height maps of the rubber membrane following single-harmonic waveform excitations at different frequencies are shown in Fig. 3(b), revealing some of the vibration modes of the circular membrane. The full dynamics of these patterns is shown in Media 3. The first three (0,1), (0,2) and (0,3) radial eigenmodes were clearly noticeable near excitation frequencies of 600 Hz, 1450 Hz and 2550 Hz, respectively, nicely matching the mathematical modeling of circular vibrating membrane [17]. Non-resonant excitation frequencies have resulted in travelling wave patterns that comprised of several eigenmodes of the membrane. These transverse waves form due to the (constant) phase difference between the different eigenmodes that are excited in the membrane. Signal-to-noise ratio (SNR) was approximately 28 dB at 600 Hz vibration (using 20 kHz line acquisition rate), estimated by calculating the ratio between the maximum and the background of the power spectrum of the oscillatory axial

#191498 - $15.00 USD Received 31 May 2013; revised 19 Jul 2013; accepted 19 Jul 2013; published 14 Aug 2013

displacement. Higher vibration frequencies often required higher line-acquisition rates, resulting in lower SNR's due to the necessary shorter exposure durations.

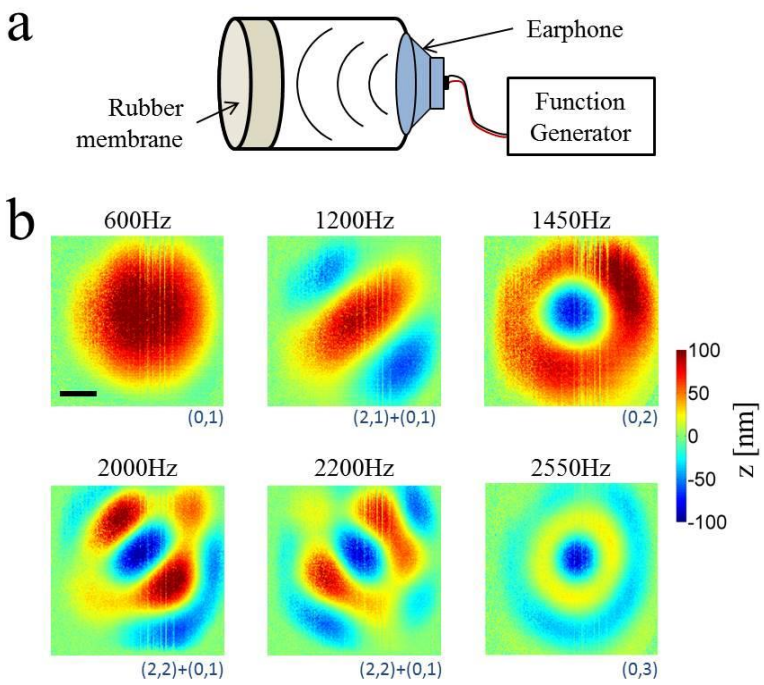

Fig. 3. (a) Schematic of the experimental arrangement for imaging vibrations of a circular rubber membrane. (b) Single frames, captured from Media 3, of different vibration modes of the membrane that was excited by single harmonic waveforms of different frequencies. Numbers at the bottom-right of each panel denote the dominant vibration modes. Scale bar represents 2 mm. Total movie duration is 1.67 ms.

In order to demonstrate vibration imaging of a biological tissue, the palm of a human volunteer was slightly pressed against a 12-mm-inner-diameter aluminum ring mounted on a linear translation stage that was driven by a piezoelectric crystal actuator [Fig. 4(a)].

The surface of the palm was imaged by our spectrally encoded interferometric system through the hole of the vibrating ring, allowing clear view of the skin surface whose edges were kept in contact with the ring inner edge throughout the measurement. Three harmonic waveforms were applied to the piezoelectric crystal at approximately ± 30 nm amplitude and frequencies of 500 Hz, 1000 Hz and 1500 Hz, resulting in tissue vibrations primarily along the optical (z) axis. Due to the radially symmetric excitation pattern and the non-resonant excitation frequency, a radially symmetric waves propagating toward the middle of the imaged circle were visible (Media 4). Selected frames separated by $\pi/3$ radian intervals are shown in Fig. 4(b) for each driving frequency. The inward-propagating waves were seen for all frequencies, having approximate velocities of 7.7 m/s, 8.1 m/s and 8.7 m/s for the frequencies 500 Hz, 1000 Hz and 1500 Hz, respectively. These velocities are in good agreement with measured velocities of shear waves (motion perpendicular to propagation direction) in tissue reported by other research groups using non-optical techniques (MRI, Ultrasound) [18, 19].

#191498 - $15.00 USD Received 31 May 2013; revised 19 Jul 2013; accepted 19 Jul 2013; published 14 Aug 2013

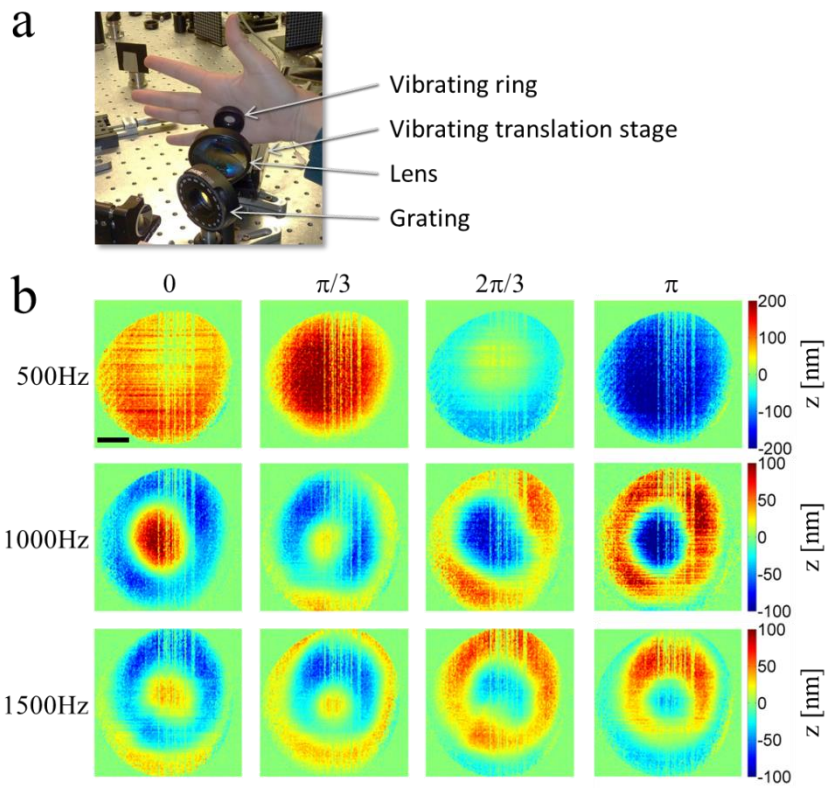

Fig. 4. (a) A photograph of the imaged palm and the distal optics of the sample arm. The experimental configuration was similar to that illustrated in Fig. 1(b). Selected frames from Media 4 of the vibrating tissue at constant phase intervals. Scale bar represents 2 mm. Total movie duration is 2 ms.

Imaging the area of a volunteer's nail fold, a relatively inhomogeneous tissue region, vibrating at 1500 Hz [Fig. 5(a)], have revealed a complex vibration pattern shown in Media 5 and in four selected frames in Fig. 5(b). Travelling waves were seen propagating from the edge of the circular field of view at different directions, where waves propagating through the relatively hard nail plate were distinctively different from those in the softer nail fold tissue, which showed a finer wave structure. The origin of the horizontal streaks that are visible in Fig. 5(b) is not entirely clear; some of the streaks are attributed to imperfection of our phase recovery algorithm at low SNR and under occasional sample movement. Some of the streaks that appear to have constant periodicity (approximately 1.6 Hz, see the two right-hand panels in Fig. 5(b)) could be related to the heartbeat of the volunteer. Vertical streaks could also be noticed in Figs. 3-5, visible mostly at low SNR conditions; these streaks are related to low amplitude wavelengths that result in less efficient phase retrievals. Using a total scan duration of 5 s and 20 kHz line rate, the SNR in imaging tissue vibrations (Figs. 4-5) was approximately 17 dB; the relatively low reflectance from the skin and the artifacts caused by tissue movement were the main factors contributing to image quality degradation.

#191498 - $15.00 USD Received 31 May 2013; revised 19 Jul 2013; accepted 19 Jul 2013; published 14 Aug 2013

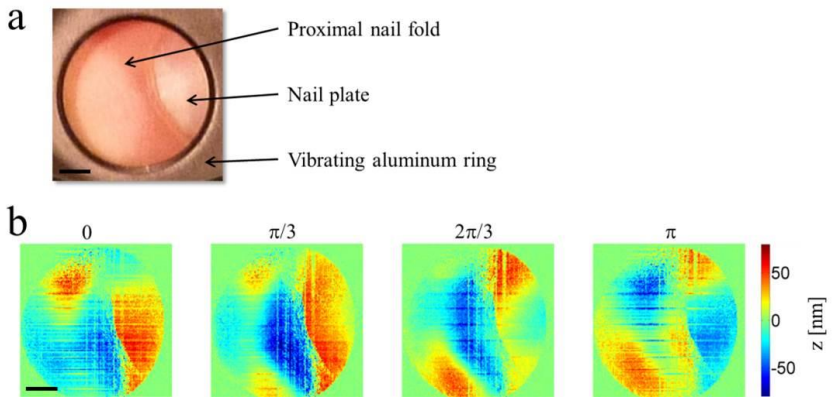

Fig. 5. (a) A photograph showing the imaged nail plate and nail fold behind the vibrating aluminum ring. (b) Selected frames from Media 5, showing wave propagation across the tissue surface. Scale bars represents 2 mm. Total movie duration is 0.67 ms.

4. Discussion

Propagation of acoustic waves in tissue could provide valuable information on its mechanical properties [20, 21]. Since tissue is inhomogeneous, high-resolution imaging is often the only way to resolve one tissue type from another. In this paper, we have developed and studied a system for two-dimensional imaging of acoustic vibrations of nanometric amplitudes in living tissue. By utilizing spatial-spectral encoding instead of mechanical scanning, our interferometric system effectively resolved axial nanometric vibrations with phase stability sufficient for measuring the entire surface displacement at high sensitivity. The absence of rapid distal scanning mechanism and the ability to use relatively simple broadband light source also helps in maintaining system simplicity, allowing future implementation of the technique using low-cost systems and compact imaging probes.

Using our spectrally encoded Doppler imaging method, the two-dimensional vibration image is acquired line-by-line, where each line contains the full vibration data, and the relative phases between subsequent lines are stitched by oversampling and post-processing the raw image. Our wave-retrieval algorithm assumes that the vibration at each location has constant amplitude and frequency throughout the measurement time; it would thus be suited for measuring continuous, steady-state oscillations and would be less efficient for observing transient events in which the excitation amplitude is not constant over time. The highest acoustic frequency that could be measured by our system was 35 kHz (limited by the maximum 70 kHz line rate of the camera), well above the maximum audible frequency (20 kHz [22]). The lower frequency limit of our system was 20 Hz, below which phase noise had significantly reduced SNR, even at high (up to 200 nm) vibration amplitudes. At frequencies between 100 Hz and 3 kHz, phase noise was the dominant noise component, limiting our amplitude detection resolution to 3 nm. We expect that sub-nanometer resolutions could be achieved in specific applications where prior knowledge of the physical properties of the vibrating subject (i.e. driving frequency and phase, surface morphology, etc.) would be used to improve data processing.

Without the need for complex and bulky two-dimensional scanning mechanisms, our optical system could be incorporated into a handheld or endoscopic device for imaging vibrations on the skin surface or inside the body. For clinical diagnosis, the proposed imaging method would be useful for measuring tissue mechanical properties at high sensitivities and high spatial resolutions. As was demonstrated in this work, an acoustic transducer could generate transverse waves across the tissue surface. Tissue regions of high stiffness, burns or small tumor nodules, for example, would be visible as regions of different propagation

#191498 - $15.00 USD Received 31 May 2013; revised 19 Jul 2013; accepted 19 Jul 2013; published 14 Aug 2013

velocities compared to the surrounding normal tissue. Another potentially important application is the evaluation of the auditory system's mechanical response to moderate-intensity sound waves, which are known to stimulate acoustic vibrations of a few nanometer amplitudes in the tympanic membrane [1]. In this application, the imaging probe could be incorporated into a handheld device (i.e. an otoscope), using a small transducer for generating the sound waves. This noninvasive measurement could provide valuable information on the mechanics and function of the tympanic membrane and the middle ear ossicles, and may offer a useful tool for diagnosing various hearing disorders.

Using a single line for measuring an entire surface also has its limitations. The system still relies on matching phases between subsequent lines, which makes it susceptible to relative motion between the probe and the tissue. We note, however, that some motion artifacts could be removed in post-processing by compensating for uniform or irregular phase shifts across the specimen. Using faster acquisition speeds, for example by using high-speed wavelength-swept sources [23], would further reduce motion artifacts and increase the upper limit of the measurable frequencies. Another challenge of the system is related to its inability to image axial surface displacements faster than a single wavelength per acquisition time (as in the case of vocal fold vibrations, for example [7]) due to phase wrapping.

In summary, we have demonstrated an effective method for imaging acoustic surface vibrations of flexible surfaces and in tissue *in vivo*, with several potential applications in clinical diagnosis. Detailed, high-resolution imaging of acoustic waves propagating in living tissue could also allow the development of new research tools, and may open new possibilities in assessing tissue mechanical properties *in situ*.

Acknowledgments

The authors thank Michal Merman for valuable discussions and technical assistance. The study was funded in part by the Israel Science Foundation grant (716/09) and by the European Research Council starting grant (239986). This work was also supported in part by the Lorry I. Lokey Interdisciplinary Center for Life Sciences and Engineering.

#191498 - $15.00 USD Received 31 May 2013; revised 19 Jul 2013; accepted 19 Jul 2013; published 14 Aug 2013